

## Electron-paramagnetic-resonance study of the (100)Si/Si<sub>3</sub>N<sub>4</sub> interface

P. Aubert

*Laboratoire Charles Fabry de l'Institut d'Optique, Boîte Postale 147, 91403 Orsay Cedex, France*

H. J. von Bardeleben

*Groupe de Physique des Solides, Universités Paris 6&7, 75251 Paris Cedex 05, France*

F. Delmotte

*Laboratoire Charles Fabry de l'Institut d'Optique, Boîte Postale 147, 91403 Orsay Cedex, France*

J. L. Cantin

*Groupe de Physique des Solides, Universités Paris 6&7, 75251 Paris Cedex 05, France*

M. C. Hugon

*Laboratoire Charles Fabry de l'Institut d'Optique, Boîte Postale 147, 91403 Orsay Cedex, France*

(Received 7 October 1998)

The (100)Si/Si<sub>3</sub>N<sub>4</sub> interface, formed by the deposition of Si<sub>3</sub>N<sub>4</sub> layers on bulk (100) Si by distributed electron-cyclotron-resonance plasma-enhanced chemical vapor deposition, has been studied by electron-paramagnetic-resonance spectroscopy. Only one interface defect, the  $P_{b0}$  center, characterized by trigonal point symmetry and principal values of the  $g$  tensor,  $g_{\parallel} = 2.0018 \pm 0.0002$  and  $g_{\perp} = 2.0089 \pm 0.0002$ , has been detected. Its area concentration is of the order of  $(2-5) \times 10^{11} \text{ cm}^{-2}$ . The characteristic defect of the (100)Si/SiO<sub>2</sub> interface, the  $P_{b1}$  center, is not observed. The Si<sub>3</sub>N<sub>4</sub> layers contain one main native bulk defect, the  $K$  center, at concentrations of  $5 \times 10^{17} \text{ cm}^{-3}$ . [S0163-1829(99)11315-8]

### INTRODUCTION

Whereas the defects at the (100) Si/SiO<sub>2</sub> interface have been studied in great detail by electrical techniques and to a lesser extent by the electron-paramagnetic-resonance (EPR) technique, the defects of the (100) Si/Si<sub>3</sub>N<sub>4</sub> interface have not yet been studied by the EPR technique up to now and the microscopic structure of the interface defects is not known. Such a study is of obvious interest for the characterization of the silicon/silicon nitride interface; but in addition it should also be useful as a reference for the (100) Si/SiO<sub>2</sub> interface, for which the defect structure is still under discussion.<sup>1-3</sup> More recently, oxynitride interfaces (100) Si/SiO<sub>x</sub>N<sub>y</sub> and nitrated Si/SiO<sub>2</sub> interfaces have also been actively studied in the search for alternative ultrathin dielectrics;<sup>1,2,4-6</sup> the knowledge of the interface defects at the silicon/silicon nitride interface is a necessary input for defect modeling in these more complex systems.

The previous defect studies at the silicon/dielectric interfaces have mainly been concerned with thermally grown SiO<sub>2</sub>. The interface structure and the interface defects have been found to depend on the crystallographic orientation of the substrate. The oxidation conditions seem to play only a minor role and modify mainly the defect concentrations. Among the three main interface orientations (111), (100), and (110) most of the EPR studies have been devoted to the (111) interface, which presents the simplest experimental case: it has only one paramagnetic interface defect—the so-called  $P_b$  center—which occurs only in one defect orientation, normal to the interface plane. At the technologically more important (100) interface two different paramagnetic

defects  $P_{b0}$  and  $P_{b1}$  coexist at comparable concentrations.<sup>7-10</sup> At the (110) interface, once again only the  $P_b$  defect has been evidenced. EPR studies of the (100) Si/SiO<sub>2</sub> interface are difficult due to reduced signal-to-noise ratios and multiple overlapping spectra. This explains why the  $g$  tensors and point symmetries of the  $P_{b0}$  and  $P_{b1}$  centers have been only recently clarified<sup>9</sup> due to the increased signal-to-noise ratios obtainable in oxidized porous silicon. It has been shown that the  $P_{b1}$  center has monoclinic  $I$  point symmetry with the principal axes of the  $g$  tensor oriented approximately along the  $[1\ 1\ 1]$ ,  $[2\ -1\ -1]$ , and  $[0\ -1\ 1]$  directions. The EPR parameters of the  $P_{b1}$  center have been confirmed very recently on bulk Si/SiO<sub>2</sub> samples, submitted to extremely high-temperature ( $>1200^\circ\text{C}$ ) vacuum annealing to increase selectively the  $P_{b1}$  center concentration.<sup>10</sup>

The microscopic structure of these defects has been established only for the  $P_b$  and  $P_{b0}$  centers: they have been convincingly attributed to a (111) oriented singly occupied silicon dangling-bond defect,  $\cdot\text{Si-Si}_3$ .<sup>11-14</sup> The microscopic structure of the  $P_{b1}$  defect is still under debate<sup>15</sup> and various models ranging from the  $\cdot\text{Si-Si}_2\text{O}$  Poindexter model, the  $\cdot\text{Si-Si-O}$  silicon dimer model initially proposed by Edwards, and more recently the original  $P_{b0}$   $\cdot\text{Si-Si}_3$  model have been considered. It now seems that the  $\cdot\text{Si-Si-O}$  silicon dimer model is the most serious candidate for  $P_{b1}$ . Further confirmation for this model comes from the very recent observation of the hyperfine structure of the  $P_{b1}$  center.<sup>16</sup> The observation of the  $P_{b1}$  center at a different (nitride) interface can be expected to further clarify this issue.

The only Si/Si<sub>3</sub>N<sub>4</sub> interface studied previously by the EPR technique is the (111) Si/Si<sub>3</sub>N<sub>4</sub> one, formed by nitration in

$\text{NH}_3$  at  $T \approx 1050^\circ\text{C}$ .<sup>17–19</sup> Paramagnetic interface defects were not observed in these samples directly after the nitration but only after post-growth high-temperature annealing ( $\geq 1050^\circ\text{C}$ ) in  $\text{N}_2$ . Only one paramagnetic defect, with EPR parameters similar to those of the  $P_b$  center, was observed. The main modification as compared to the oxide case was the increase in the EPR linewidth—5.5 G as compared to 2.1 G (first derivative peak-peak width at X band for  $B \parallel [001]$ ). Unfortunately the impact of the high-temperature annealing on the interface quality remains unclear: it is just either simple depassivation of existing  $P_b$  centers or does it lead to structural modifications of the interface.

We present here the results of an EPR study of interface and bulk defects in (100)Si/Si<sub>3</sub>N<sub>4</sub> formed by the deposition of thin ( $\sim 100$  Å) Si<sub>3</sub>N<sub>4</sub> layers on bulk (100) Si by the distributed electron-cyclotron-resonance plasma-enhanced chemical vapor deposition (DECR-PECVD) technique. The composition of the Si<sub>3</sub>N<sub>4</sub> layer has equally been characterized by photoelectron spectroscopy (XPS).

### EXPERIMENT

The silicon nitrides films have been deposited by DECR-PECVD technique from ultrapure SiH<sub>4</sub> and N<sub>2</sub> gas mixtures on both *n*- and *p*-type doped (100) Si substrates. Before deposition the substrates received a standard RCA cleaning. The deposition conditions had been optimized previously:<sup>20</sup> they correspond to a gas flow ratio N<sub>2</sub>/SiH<sub>4</sub> of 19, a total flow rate of 20 sccm, a pressure to 0.3 Pa, and a microwave power of 1500 W. The deposition temperature was estimated to 100 °C. For these conditions the deposition rate is  $\sim 20$  Å/min. Films with thickness between 20 and 600 Å have been grown. After the film deposition the samples were thermally annealed at 450 °C for 30 min in an argon gas atmosphere. As shown in Ref. 20, this annealing leads to the formation of a high-quality interface with midgap interface state densities in the  $6 \times 10^{10}$  eV<sup>-1</sup> cm<sup>-2</sup> range and a fixed charge density of  $1 \times 10^{12}$  cm<sup>-2</sup>.

The film composition has been analyzed by nuclear microanalysis: it corresponds to total concentrations of  $[\text{N}] = (5.2 \pm 0.2) \times 10^{22}$  at/cm<sup>3</sup>,  $[\text{Si}] = (3.6 \pm 0.1) \times 10^{22}$  at/cm<sup>3</sup>,  $[\text{H}] = (1 \pm 0.5) \times 10^{22}$  at/cm<sup>3</sup>,  $[\text{O}] = (0.2 \pm 0.06) \times 10^{22}$  at/cm<sup>3</sup>. This corresponds to a nominal stoichiometry of  $[\text{N}]/[\text{Si}] = 1.44$ , i.e., the films are slightly nitrogen-rich.

The XPS measurements have been performed with a non-monochromatic Mg *K*α source and the photoelectrons were detected for two different (14° and 64° from normal) escape angles. The Si 2*p*, N 1*s*, and O 1*s* spectra were analyzed. The two spin-orbit components of the Si 2*p* spectra were decomposed assuming a spin-orbit coupling constant of 0.61 eV and a ratio of  $I_{\text{Si}2p_{1/2}}/I_{\text{Si}2p_{3/2}} = 0.5$ .

For the EPR measurements, samples with a typical size of  $2 \times 20$  mm<sup>2</sup> were prepared. The X-band (9.4 GHz) EPR measurements were performed both at low temperature (4 and 32 K) as well as at room temperature. For the determination of the *g* values the microwave frequency was measured by a frequency counter and the magnetic field was determined by a microprocessor controlled Hall probe (Bruker BH15). The *g* factors were in addition calibrated at low temperature relative to a Si:P standard sample ( $g = 1.9985$ ) and at room temperature relative to a MgO:Mn

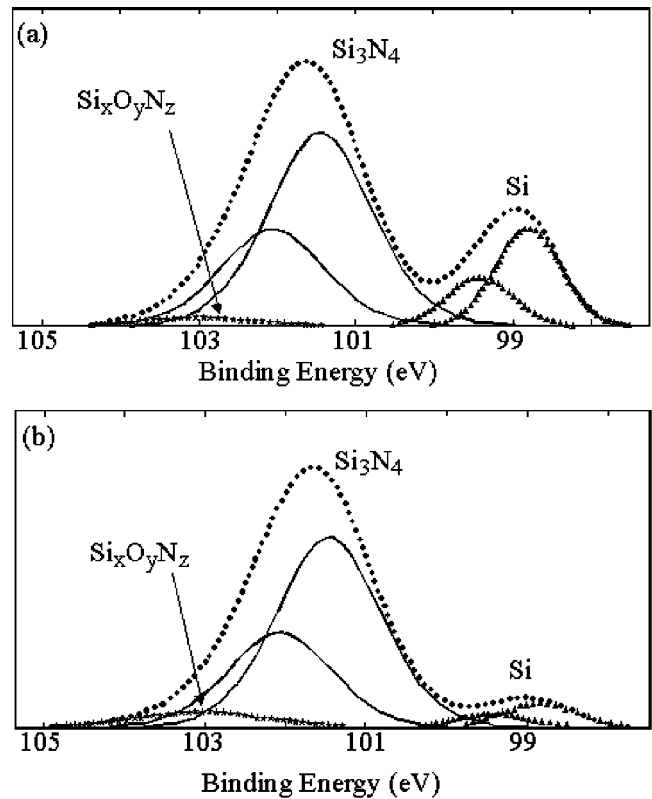


FIG. 1. XPS spectra of (100)Si/Si<sub>3</sub>N<sub>4</sub> for normal (a) and 40° photoelectron escape angles; layer thickness of 20 Å.

sample. The error is estimated to  $\Delta g = \pm 0.0002$ . The magnetic field was modulated at 100 kHz with amplitudes of typically 2 G. The EPR spectra were taken under slow adiabatic passage conditions to exclude line-shape distortions generally encountered when working under rapid passage conditions or in second-harmonic detection. The spectra were typically iterated  $\sim 10$  times to improve the signal-to-noise ratio. The total angular-dependent EPR spectra were then analyzed by a computer-assisted decomposition in their different components. For each component of the spectrum the line shapes (Gauss, Lorentz, and Voigt), the position, width, and amplitude were determined. The absolute spin concentrations were obtained by comparison with an Al<sub>2</sub>O<sub>3</sub>:Cr spin standard sample purchased from the National Bureau of Standards.

### XPS STUDY OF THE Si/Si<sub>3</sub>N<sub>4</sub> INTERFACE

The (100)Si/Si<sub>3</sub>N<sub>4</sub> interfaces and the composition of the Si<sub>3</sub>N<sub>4</sub> layer were first characterized by a series of XPS measurements. The core-level spectra of Si 2*p*, N 1*s*, and O 1*s* were measured in samples with thin (20 Å) or thick (200 Å) nitride films. To probe the localization of the small oxygen contamination in the 20 Å thin Si<sub>3</sub>N<sub>4</sub> layers, XPS measurements for two different escape angles were taken.

A typical Si 2*p* XPS spectrum for a 20-Å-thick nitride is shown in Fig. 1(a). It is composed of two main spectra at 99 and 101.6 eV, which are decomposed in the usual spin-orbit doublets (Table I). From their energy positions they are attributed to Si in silicon (Si<sup>0</sup>) and Si in Si<sub>3</sub>N<sub>4</sub> (Si<sup>4+</sup>), respectively. The chemical shift of 2.7 eV is characteristic of Si in

TABLE I. Parameters of the Si  $2p$  XPS spectra of (100) Si/Si<sub>3</sub>N<sub>4</sub>; layer thickness 20 Å, detection angle 14° from normal.

Transition	$E$ (eV)	FWHM (eV)	$L/G$ (%)	$I$ (%)
Si <sup>0</sup> $2p_{3/2}$	98.81	0.95	0.3	14.9
Si <sup>0</sup> $2p_{1/2}$	99.42	0.95	0.3	7.5
Si <sup>4+</sup> $2p_{3/2}$	101.46	1.58	48.9	50.5
Si <sup>4+</sup> $2p_{1/2}$	102.07	1.58	48.9	25.2
Si <sup>4+</sup>	103.06	1.38	8.3	1.9

Si<sub>3</sub>N<sub>4</sub>. In the case of a SiO<sub>2</sub> oxide layer, the corresponding shift is 3.9 eV and if the layer were of the SiO<sub>x</sub>N<sub>y</sub> oxynitride type intermediate shifts should be found.<sup>21,22</sup>

The fit reveals an additional small intensity (2.8%) peak at 103 eV, which we attribute to Si<sup>4+</sup> in SiO<sub>2</sub>. Its low intensity does not allow a decomposition into the two spin-orbit components. To probe the depth localization of this oxide, we have measured the intensity of this peak equally for a detection angle of 64° from normal incidence. As seen in Fig. 1(b), it increases from 2.8% to 4%. This result indicates that the oxide layer is mainly situated at the surface of the nitride layer. It confirms ion beam analysis, which had already revealed that a thin oxide layer is formed at the outer surface of the nitride, when the layer is exposed to ambient conditions. The absence of an oxide layer at the interface is due to the action of H<sub>2</sub> in the ECR plasma, which is known to take off any residual native oxide surface layer.<sup>23</sup>

In the previous XPS and EPR study of the (111)Si/Si<sub>3</sub>N<sub>4</sub> interface,<sup>19</sup> obtained by thermal nitration in NH<sub>3</sub>, in addition to the surface oxide layer a thin oxide layer at the interface had been observed. Its presence is certainly of importance for the nature and concentration of the interface defects. It had been attributed to an insufficient substrate preparation, in which the native oxide layer had not been fully removed. Under our DECR PECVD deposition conditions only 2.8 at. % of oxygen are incorporated in the layer and the interface does not contain a residual native silicon oxide layer.

## EPR RESULTS

Typical EPR spectra of a  $p$ -type (100)/Si<sub>3</sub>N<sub>4</sub> sample for different orientations of the magnetic field between  $B \parallel [001]$   $B \parallel [110]$  are shown in Fig. 2; they were taken at a temperature of 4 K and a microwave power of 2 μW. The spectra show a strong angular dependence. A detailed analysis of the angular variation of the spectrum measured at different microwave powers, temperatures, and for different dielectric layer thickness demonstrates that the total EPR spectrum can be modeled as the superposition of two isotropic one-line spectra and one anisotropic spectrum of trigonal symmetry (Fig. 3). Based on their  $g$  factors, linewidths, and line shapes, the spectra are attributed to the  $K$  center in the nitride layer, the silicon dangling-bond defect, and the  $P_{b0}$  interface defect, respectively (Fig. 3). The total spectrum is quantitatively decomposed for all orientations in the sum of the EPR spectra of these three different defects. Figures 4 and 5 show this decomposition for the three principal orientations of the magnetic field (Fig. 4) and as a function of microwave power

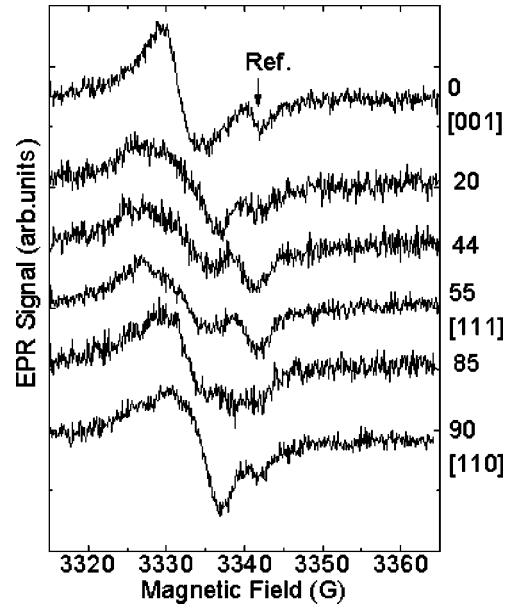


FIG. 2. EPR spectra of (100)Si/Si<sub>3</sub>N<sub>4</sub> as a function of the orientation of the magnetic field;  $T=4$  K; the line (↓) is an isotropic reference line from the sample holder.

(Fig. 5) in the case of a  $p$ -type substrate. The computer-assisted decomposition is straightforward, as the absolute intensities of each line as well as the angular variation of the  $P_{b0}$  center linewidth put strong constraints on this decomposition. The slow passage conditions under which the EPR spectra were recorded are essential to avoid line-shape distortions, which would render the decomposition impossible. The  $P_{b1}$  defect, the characteristic interface defect of the (100)Si/SiO<sub>2</sub> interface, is not observed.

The same three spectra are equally observed with unchanged parameters at 32 K (Fig. 6); due to different relaxation times for the three defects the apparent relative intensities are modified. In the  $n$ -type samples the phosphorus spectrum from the substrate is in addition observed at 32 K.

At room temperature the  $P_{b0}$  center and the Si db signal are still well observed at mW microwave powers, whereas the  $K$  center, which has shorter relaxation times, is no longer observed (Fig. 7).

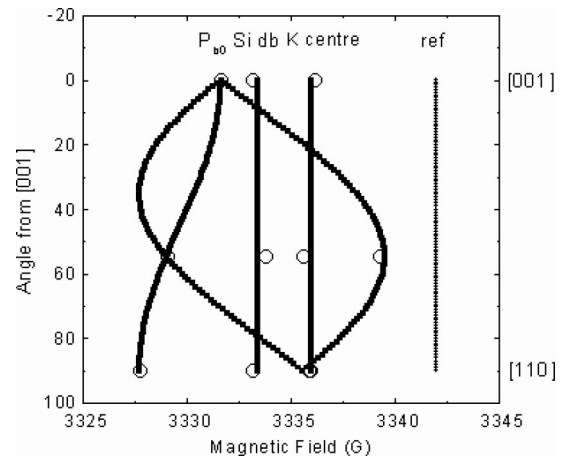


FIG. 3. Angular variation of the EPR spectra of the  $P_{b0}$  center, Si dangling bond, and the  $K$  center; simulation (line), experimental points (circles).

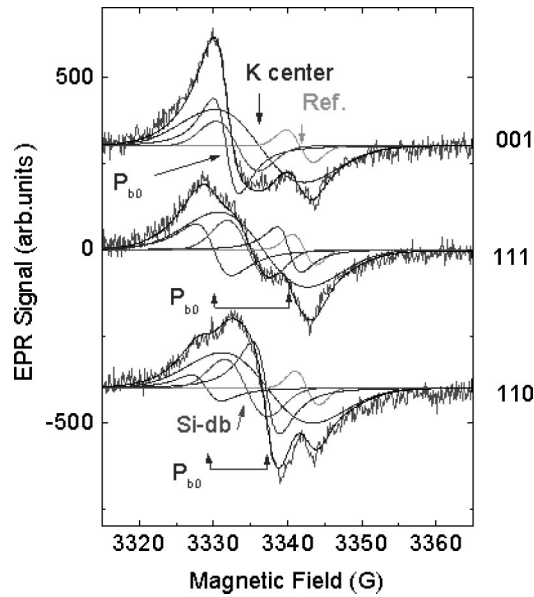


FIG. 4. Decomposition of the total EPR spectrum in the  $P_{b0}$ , Si db, K center, and reference lines; the experimental spectrum, the individual lines, and their sum line are shown for three magnetic field orientations;  $T=4$  K.

Identical EPR spectra were observed for both the  $n$ -type and  $p$ -type conducting substrates.

#### $P_{b0}$ INTERFACE DEFECTS

The anisotropic part of the EPR spectrum is well simulated by a spin  $S=\frac{1}{2}$  defect with trigonal point symmetry and principal values of the  $g$  factor of  $g_{\parallel}=2.0018+0.0002$  and  $g_{\perp}=2.0089+0.0002$ . The (X-band) line shape is Lorentzian with a peak-to-peak first derivative linewidth varying between 3.2 and 4.8 G for  $B\parallel[111]$  and  $B\perp[111]$ , respectively (Fig. 4). The  $g$  tensor and the  $C_{3v}$  symmetry identify this defect as the  $P_{b0}$  center. The principal values of the  $g$  tensor

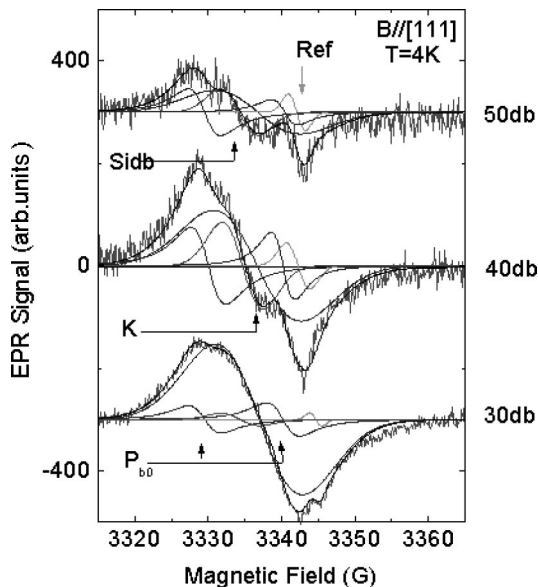


FIG. 5. Decomposition of the EPR spectra of (100) Si/Si<sub>3</sub>N<sub>4</sub> for three different microwave powers;  $B\parallel[111]$ ,  $T=4$  K; the experimental spectrum, the individual lines, and their sum line are shown.

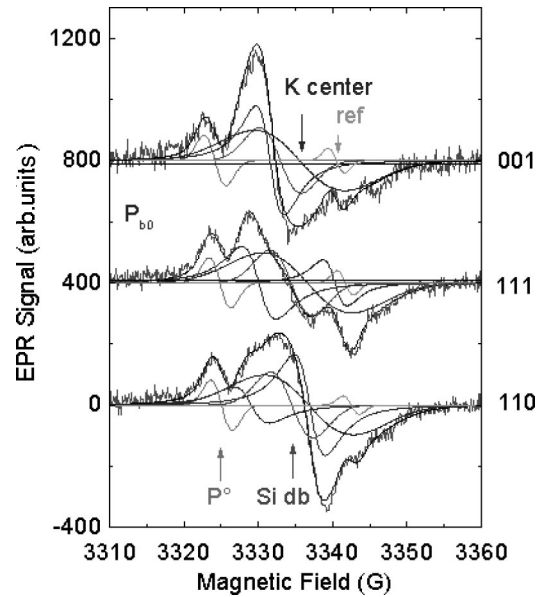


FIG. 6. Decomposition of the total EPR spectrum taken at  $T=32$  K in the  $P_{b0}$ , Si dB, K center, and reference lines; experimental spectrum, sum line, and individual lines are shown for three magnetic field orientations. As the substrate is  $n$ -type doped and we observe in addition the two EPR lines from the phosphorus donor; only the low field phosphorus line is visible in this field range.

are very close to those previously observed for the  $P_{b0}$  center at the (100)Si/SiO<sub>2</sub> interface and the  $P_b$  centers at the (111)Si/SiO<sub>2</sub> and (111)Si/Si<sub>3</sub>N<sub>4</sub> interfaces (Table II). This result is surprising as the nitride interface due to the different coordination of N as compared to O might be expected to contain different interface defects. This result could be understood if the defect structure around the Pb defect is more extended than generally assumed, i.e., one unbonded Si atom with all nearest neighbors in the interface plane bonded to

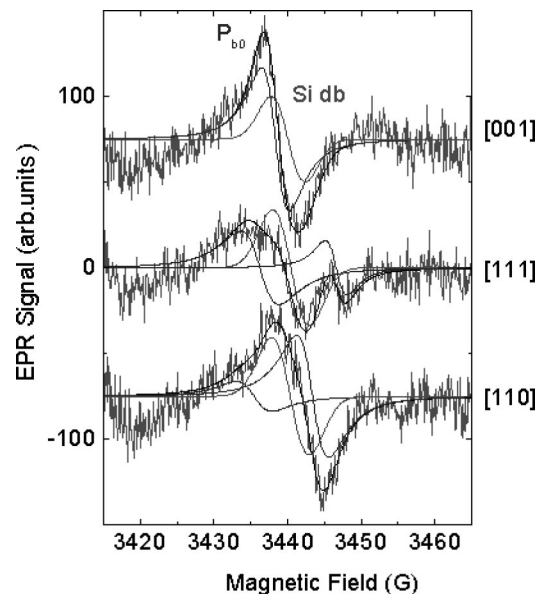


FIG. 7. Room-temperature spectra of an  $n$ -type (100)Si/Si<sub>3</sub>N<sub>4</sub> layer and the decomposition in  $P_{b0}$  and Si db lines for three field orientations: the experimental spectrum, the  $P_{b0}$  and Si db lines, as well as their sum line are shown.

TABLE II. Comparison of principal  $g$  values of the trigonal  $P_b, P_{b0}$  centers at various nitride and oxide interfaces.

Defect	$P_b$	$P_b$	$P_{b0}$	$P_{b0}$	$P_b, P_{b0}$
type of interface	(111) Si/SiO <sub>2</sub>	(111) Si/Si <sub>3</sub> N <sub>4</sub>	(100) Si/SiO <sub>2</sub>	(100) Si/Si <sub>3</sub> N <sub>4</sub>	porous Si
$g_{\parallel}$	2.0014	2.0015	2.0019	2.0018	2.0017–2.0020
$g_{\perp}$	2.0088	2.0081	2.0081	2.0089	2.0082–2.0090
oxidation conditions	standard oxide	1120 °C NH <sub>3</sub> + 1200 °C anneal N <sub>2</sub>	170 °C oxide	100 °C deposited + 450 °C anneal	varies with porosity, oxidation conditions
Reference	7	17–19	10	this work	9 and 24

oxygen atoms. Indeed the electron nuclear double resonance (ENDOR) studies of the Pb centers<sup>24,25</sup> in oxidized porous silicon had shown a distribution of hydrogen passivated Si interface atoms surrounding the paramagnetic Pb center. Such a structure could explain that we observe in all cases the same basically “isolated” paramagnetic Si dangling-bond defect.

Whereas this explanation is easy to conceive for (111) oriented interfaces, the case of (100) interfaces is certainly more complex: rigorously, at a nonreconstructed (100) Si surface, Si dangling-bond defects of the form Si<sub>3</sub>-Si· (i.e.,  $P_{b0}$  centers) with exactly trigonal point symmetry should not occur due to the nonequivalence of the three Si bonding atoms (Fig. 8). Even in the original Poindexter model for  $P_{b0}$ ,<sup>11</sup> which places the  $P_{b0}$  center in a transition layer between Si and SiO<sub>2</sub>, the three Si nearest-neighbor atoms are not equivalent. Further, in this model an oxygen atom is situated at a nearest-neighbor distance from the Pb center, which is difficult to reconcile with the weak <sup>17</sup>O hyperfine interaction observed for this defect.<sup>14,24</sup> As concerns the orientation of the symmetry axis of the  $P_{b0}$  center, only two directions are possible in a given (100) plane, whereas four orientations are in general experimentally observed. Thus the

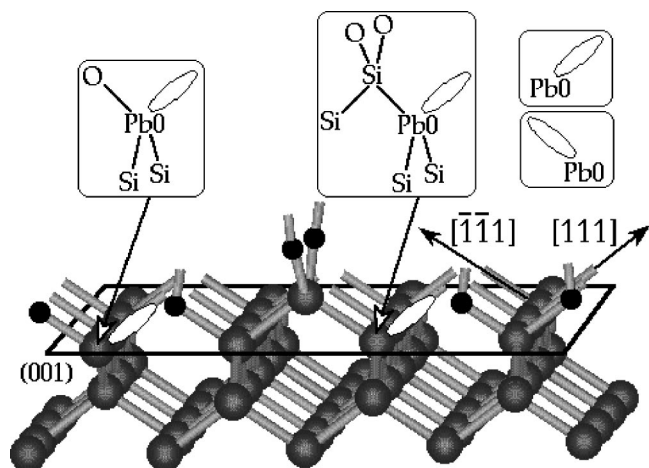


FIG. 8. (100) Si interface plane with two possible Si dangling-bond configurations, the center one corresponding to the Poindexter model; the small black circles represent nitrogen or oxygen atoms; both configurations lead to nonequivalent first-nearest-neighbor atoms for the Pb center; only two orientations for the nonbonded  $sp^3$  orbitals of the interface atom are possible.

presence of the  $P_{b0}$  defect at the (100) interface with, in particular, nearly unchanged spin Hamiltonian parameters as compared to (111)Si/SiO<sub>2</sub> interfaces—including the silicon central hyperfine and super hyperfine tensors—is difficult to conceive. We have recently argued<sup>3,14</sup> that a local (111) facet formation at (100)Si/SiO<sub>2</sub> interfaces is a probable explanation (see Fig. 9), which should be considered in the interface modeling.<sup>26</sup> We will come back to this point in the Discussion.

The linewidth of the  $P_{b0}$  center and its variation with the magnetic field orientation reflect in addition a distribution in the microscopic configurations of this defect. It has been shown previously in the oxide case by EPR measurements at different microwave frequencies that the linewidth increases proportionally to the microwave frequency; it is thus due to a nonresolved  $g$ -tensor distribution. The observed anisotropy with  $\Delta g_{\parallel} < g_{\perp}$  has been explained by first- and second-order effects of variations in bond length and angles on the  $g_{\perp}$  and  $g_{\parallel}$  values, respectively. In the case of Si<sub>3</sub>N<sub>4</sub> the superhyperfine (SHF) interaction with the nuclear spins of <sup>14</sup>N, <sup>15</sup>N can give rise to an additional isotropic broadening. The linewidth of  $\Delta B_{\parallel} = 3.2$  G measured here must be compared to the typical value of 1.6 G observed in the case of silicon oxide interfaces. The linewidth shows only a very weak temperature dependence: we have compared the linewidths for the same sample at 4, 32, and 293 K. For  $B \parallel [111]$  we find, respectively, values of 3.4, 3.2, and 3.0 G. To distinguish the contributions to the linewidth by the SHF interaction with <sup>14</sup>N, <sup>15</sup>N nuclei from that of increased interface roughness at the nitride interface ( $g$ -tensor distribution), additional EPR measurements at higher frequencies are required.

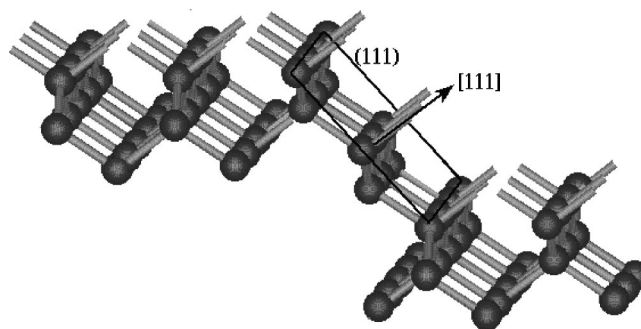


FIG. 9. (100) Si interface plane with a (111) facet plane at a two-atomic-layer step.

The concentrations of the  $P_{b0}$  centers in the 450 °C annealed samples are between  $(5-7) \times 10^{11}$  cm<sup>-2</sup>. This concentration can be compared with those determined by electrical measurements if we take into account that the Pb centers due to variation in their local environments gives rise to an  $\sim 0.2$  eV wide distribution of the electrical levels. As in EPR, the total Pb center concentration irrespective of the particular position of the electrical  $-/0$  level in the gap is seen, and the EPR concentration of Pb centers is of course higher than the minimum value of  $D_{it}$  at midgap generally cited in electrical characterizations. The value of  $(5-7) \times 10^{11}$  cm<sup>-2</sup> is thus in agreement with the one deduced from the electrical  $C(V)$  measurements were the minimum interface defect density at midgap was measured as  $6 \times 10^{10}$  eV<sup>-1</sup> cm<sup>-2</sup>.<sup>20</sup>

### THE $K$ CENTER

The EPR spectrum of the  $K$  center is characterized by an isotropic  $g$  factor of  $g = 2.0037 + 0.0002$ , a linewidth of  $(12.0 \pm 0.5)$  G, and a Gaussian line shape. The  $K$  centers, which are bulk defects, have been previously identified as a threefold-coordinated Si dangling-bond center, where the Si atom is bonded with one, two, or three N atoms, respectively.<sup>27,28</sup> The  $K$  centers were mainly studied in thick, amorphous hydrogenated Si<sub>3</sub>N<sub>4</sub> layers deposited by CVD techniques from SiH<sub>4</sub> and NH<sub>3</sub> or N<sub>2</sub>O gases. In CVD deposited layers this center is not observable by EPR in the as-deposited state, but only after uv illumination. Photoexcitation with energies above 5 eV generates free electrons and holes, the capture of which transforms the  $K$  center in a paramagnetic charge state. The situation is different for PECVD prepared layers, where they are observed without any post-deposition uv illumination. It is supposed that the uv light emitted by the plasma generates paramagnetic  $K$  centers during the entire deposition process. This situation is analogous to the one of the PECVD deposited SiO<sub>2</sub> layers, where the paramagnetic positively charged  $E'$  center is equally observed in the as-deposited dielectric layer.<sup>29</sup>

The  $g$  factor of the  $K$  center is dependent on the local bonding configuration Si- $X_3$  and can thus be used as a probe for the composition of the nitride layer: indeed, studies of this defect in silicon nitride layers of different compositions Si <sub>$x$</sub> N <sub>$y$</sub>  have shown<sup>30</sup> that for the  $K$  centers in stoichiometric Si<sub>3</sub>N<sub>4</sub> layers where the nearest-neighbor configuration of the  $K$  center is \*Si-N<sub>3</sub>, the  $g$  factor is 2.0030. Substitution of one of the N neighbors by a silicon atom (\*Si-N<sub>2</sub>Si) increases the  $g$  factor to 2.0033; further substitution leads to the  $g$  factors of 2.0040 (\*Si-NSi<sub>2</sub>) and the \*Si-Si<sub>3</sub>Si dangling-bond defect has its  $g$  factor of 2.0055. The linewidth depends also on the configuration due to the (generally nonresolved) hyperfine interaction with the <sup>14</sup>N ( $I=1$ ) and <sup>15</sup>N ( $I=1/2$ ) nuclei: whereas the Si-Si<sub>3</sub> center has a linewidth of typically  $(6 \pm 1)$  G, this width increases to  $\sim 13$  G for Si-N<sub>3</sub>. These assignments based on experimental results were confirmed by the modeling of the  $g$  tensor for the different defect complexes.<sup>28</sup> The  $g$  factor of 2.0039 demonstrates that the  $K$  centers observed in our layers have a configuration ·Si-Si<sub>2</sub>N; the occurrence of such defects in N-rich films is certainly related to the low deposition temperature.

In the previous EPR study on thermally nitrated (111)Si/Si<sub>3</sub>N<sub>4</sub> (Refs. 17–19) a quite different EPR spectrum

characterized by a  $g$  value of  $g = 2.0028$  and a peak-to-peak linewidth of 2.4 G, observed without any uv illumination, had been attributed to the  $K$  center. However, given the multiple results for the  $K$  centers now available, this attribution seems to be erroneous. Indeed, the small linewidth and its frequency dependence seem more to be in favor of a 19° Pb center, often observed in samples with rough interfaces.

The concentration of the  $K$  centers in the 100-Å-thick Si<sub>3</sub>N<sub>4</sub> layer not submitted to post growth uv excitation is  $(3-5) \times 10^{17}$  cm<sup>-3</sup>.

### Si DANGLING-BOND DEFECT

In addition to the  $K$  center we observe equally a second isotropic EPR spectrum, characterized by a  $g$  factor of 2.0055, a linewidth of  $(5.5 \pm 0.5)$  G, and a Gaussian line shape. These parameters clearly identify this defect as a ·Si-Si<sub>3</sub> defect in an amorphous matrix. Two probably coexisting sources for this defect can be considered: (i) Si db defects at the amorphous surface of the cleavage planes of the EPR samples as well as (ii) ·Si-Si<sub>3</sub> volume defects in the Si<sub>3</sub>N<sub>4</sub> layer. This defect is well known to be formed on cleaved silicon surfaces and can be eliminated by a treatment in boiling hydrazine. We did not want to apply this treatment to our thin Si<sub>3</sub>N<sub>4</sub> layers to avoid any structural modification. We have found that an additional 450 °C annealing, which oxidizes these cleavage surfaces, strongly reduces the concentration of the Si db centers. It cannot be excluded that the remaining Si db defects are intrinsic defects of the Si<sub>3</sub>N<sub>4</sub> layer but further separate studies are necessary to assign these defects.

### DISCUSSION

The DECR-PECVD deposition techniques allow us to deposit silicon nitrides films of various stoichiometries, which range from slightly nitrogen-rich  $[N]/[Si]=1.44$  over stoichiometric composition  $[N]/[Si]=1.33$  to silicon-rich  $[N]/[Si]=1.2$ . These films contain in addition high amounts of hydrogen in the 10–18 at. % range. The physical properties of the film and the interface structure depend on the stoichiometry. Our deposition conditions were chosen to optimize the electrical properties of the nitride layer; for films with a N/Si ratio of 1.44 we obtain minimum fixed nitride charges ( $1.6 \times 10^{12}$  cm<sup>-2</sup>), a minimum interface defect density of  $6 \times 10^{10}$  eV<sup>-1</sup> cm<sup>-2</sup>, and high critical fields.

The first important result obtained in this study is the nonobservation of the  $P_{b1}$  center, the defect generally thought to be characteristic of all (100)Si/SiX-type interfaces. As we have been able to measure the interface defects up to room temperature, it seems clear that long relaxation times, which can render low-temperature EPR measurements of paramagnetic defects difficult, are not the reason for the nonobservation of  $P_{b1}$ . It follows, therefore, that  $P_{b1}$  centers are not characteristic defects of the (100)Si/dielectric interfaces, but of the (100)Si/SiO<sub>2</sub> interface. Their presence must be related to the oxygen bonding configuration in the transition layer close to the interface. This result is qualitatively confirmed by DLTS measurements on similarly prepared (100)Si/silicon nitride structures, which had revealed only one DLTS peak at  $E_c-0.25$  eV, the characteristics of which

TABLE III. X-band peak-to-peak linewidths at  $T=4$  K for  $P_b$  and  $P_{b0}$  centers at various nitride and oxide interfaces.

defect	$P_b$	$P_b$	$P_b$	$P_{b0}$	$P_{b0}$
type of interface	(111) Si/SiO <sub>2</sub>	(111) Si/Si <sub>3</sub> N <sub>4</sub>	(111) Si/Si <sub>3</sub> N <sub>4</sub>	(100) Si/SiO <sub>2</sub>	(100) Si/Si <sub>3</sub> N <sub>4</sub>
$\Delta B_{\parallel}pp$ (G)	1.8	5.5	5.0–6.8	2.7	3.2
$\Delta B_{\perp}pp$ (G)	3.3	5.5	6.0–7.3	3.7	4.8
nitridation conditions	thermal O <sub>2</sub> at 920 °C + anneal at 835 °C under vacuum	thermal NH <sub>3</sub> at $T_N=1120$ °C + anneal at $T_N$ under N <sub>2</sub>	thermal NH <sub>3</sub> at $T_N=1120$ °C + anneal at $T_N$ under N <sub>2</sub>	thermal O <sub>2</sub> at 950 °C + anneal at 650 °C under vacuum	deposited at 100 °C+ + anneal at 450 °C
Reference	19	17 and 18	19	6	this work

correspond well to the  $P_{b0}$  defect at the Si/SiO<sub>2</sub> interface. No DLTS peak attributable to  $P_{b1}$  had been detected.<sup>31</sup>

The only paramagnetic interface defect observed is the  $P_{b0}$  center with trigonal point symmetry with a symmetry axis parallel to [111]. Its  $g$  tensor and hyperfine interactions (determined for the oxide case only) are in good agreement with the model of a paramagnetic Si atom bonded to three equivalent first-nearest-neighbor Si atoms. This configuration is the natural one for nonbonded interface atoms at the (111) oriented interface and suggests the idea of a partially (111) faceted (100) Si interface. Such a model had already been proposed previously on the basis of electron microscopy results<sup>32</sup> and from the EPR studies in porous silicon.<sup>3,14</sup> The experimentally determined intensity of each of the four  $P_{b0}$  EPR lines allows us to develop this model further. Assuming the  $P_{b0}$  centers to be localized on (111) facets, we can estimate the relative area of each of the four differently oriented (111) facets from the intensity of each  $P_{b0}$  line. The experimental results show that the four facet orientations do not occur with the same probability. For the rotation of the magnetic field in the (110) plane two of the EPR lines are degenerate and in the case of random distribution we should observe a 1:2:1 intensity distribution of the EPR lines. However, we do observe systematically values of 2:1:1 (Figs. 3–5), which indicates that the facets are not randomly oriented. In fact, such a distribution corresponds to an ensemble of parallel oriented facets, which outnumber the perpendicular oriented facets by 3:1. Such a situation would arise naturally if parallelly oriented steps had been formed at the interface in the initial deposition stage.

The principal values of the  $g$  tensor are rather insensitive to the interface orientation and chemical composition of the dielectric (Table II). This finding is in agreement with an extended defect structure around the Pb defects, which results in basically “isolated” Si dangling-bond defects. The linewidths of the  $P_{b0}$  center give additional information about the microscopic configuration around the defects. It has been established for the  $P_{b0}$  center at the oxide interface that in addition to inhomogeneous broadening due to nonresolved hyperfine interaction with <sup>29</sup>Si nuclei the linewidth is determined by a nonresolved  $g$ -tensor distribution. The  $g$ -tensor distribution reflects the different local environments of the  $P_{b0}$  center, in agreement with the electrical measurements, which have shown an  $\sim 0.2$  eV wide level distribution

around the mean value of  $E_c - E_T$  and  $E_v + E_T$ , for the  $-/0$  and  $0/+$  charge states. The minimum  $g$ -factor distribution is observed for  $B_{\parallel}[111]$  where (X band first derivative peak-to-peak) linewidths of  $(1.5 \pm 0.2)$  G are found (Table III). In our (100) Si/Si<sub>3</sub>N<sub>4</sub> samples this value is increased to  $(3.2 \pm 0.2)$  G and for thermal nitrides at (111) Si this value is even higher with 6 G. It has been already argued in Ref. 19 that this increase is due to larger  $g$ -tensor distributions and not to the additional hyperfine interaction with the <sup>14</sup>N, <sup>15</sup>N nuclei. We observe therefore an increase in interface roughness from SiO<sub>2</sub> over deposited nitrides to thermally grown nitrides.

The concentration of the  $P_{b0}$  centers is in the mid  $10^{11}$  cm<sup>-2</sup> range after 450 °C annealing. This value is lower than the concentration of  $P_b$  centers found in the case of thermally grown (111) Si/Si<sub>3</sub>N<sub>4</sub> interfaces, where concentrations in the  $10^{13}$  cm<sup>-2</sup> range have been found. The decrease in the interface defect concentration is similar to the oxide case, where (100) oriented interfaces have about fibers times lower defect concentrations than (111) oriented ones. For ECR-PECVD grown (100) Si/Si<sub>3</sub>N<sub>4</sub> samples the minimum interface state density  $D_{it}$  depends in addition on the stoichiometry of the nitride layers: for nitrogen-rich layers a change in the composition from  $[N]/[Si]=1.4$  to 1.5 leads to a monotonous increase in the  $D_{it}$  from 2 to  $20 \times 10^{11}$  eV<sup>-1</sup> cm<sup>-2</sup>.<sup>31</sup> This variation is correlated with the concentration of N-H bonds, and a model which links the presence of N-H bonds near the interface with the Pb center formation has been proposed.<sup>33</sup>

Whereas in LPCVD Si<sub>3</sub>N<sub>4</sub> layers deposited at 600 °C the  $K$  centers have the expected coordination  $\cdot\text{Si-N}_3$  ( $g$  factor  $g=2.0030$  and linewidth  $\Delta B_{pp}=13$  G, their coordination in low-temperature PECVD layers with a stoichiometric composition or slightly N rich is  $\cdot\text{Si-N}_2\text{Si}$ .<sup>27,28</sup> The  $K$  centers, which are paramagnetic in the neutral charge state, can trap both electrons and holes.<sup>34</sup> The concentration observation before uv illumination is thus related to the electrical compensation. Electron injection studies in our layers<sup>35</sup> show a lower limit of electron traps of  $5 \times 10^{17}$  cm<sup>-3</sup>, which correlates well with the concentration of  $K$  centers measured by EPR. Thus the  $K$  centers are the dominant electron traps in these layers.

## CONCLUSIONS

The interface obtained by low-temperature deposition of Si<sub>3</sub>N<sub>4</sub> on (100) Si is characterized by the presence of only

one paramagnetic interface defect, the  $P_{b0}$  center, at concentrations of  $5 \times 10^{11} \text{ cm}^{-2}$ . The  $P_{b1}$  center, systematically observed at (100)Si/SiO<sub>2</sub> interfaces, is absent at this interface. The lower linewidth of the  $P_{b0}$  center as compared to the one at the (111)Si/thermal nitride interface indicates a lower interface roughness. The layers, which are of average com-

position  $[N]/[Si]=1.44$ , contain one main electron trap, the  $K$  center, in the configuration  $\cdot\text{Si-N}_2\text{Si}$ .

#### ACKNOWLEDGMENTS

The authors thank J. Olivier (Thomson CSF-LCR) for the XPS measurements and helpful discussions.

- <sup>1</sup>*The Physics and Chemistry of SiO<sub>2</sub> and the Si-SiO<sub>2</sub> Interface-3*, edited by H. Z. Massoud, E. H. Poindexter, and C. R. Helms (The Electrochemical Society, Los Angeles, 1996).
- <sup>2</sup>J. H. Stathis, E. Cartier, A. H. Edwards, and E. H. Poindexter, in *Silicon Nitride and Silicon Dioxide Thin Insulating Films IV*, edited by M. J. Deen, W. D. Brown, K. B. Sundaram, and S. I. Raider (The Electrochemical Society, Pennington, NJ, 1997), p. 259.
- <sup>3</sup>H. J. von Bardeleben and J. L. Cantin, *Braz. J. Phys.* **27**, 314 (1997).
- <sup>4</sup>Z. Q. Yao, H. B. Harrison, S. Dimitrijevic, and D. Sweatman, *Appl. Phys. Lett.* **64**, 3584 (1994).
- <sup>5</sup>Z. Ying and G. Lucovsky, *J. Vac. Sci. Technol. B* **13**, 1613 (1995).
- <sup>6</sup>H. J. von Bardeleben, J. L. Cantin, L. G. Gosset, J. J. Ganem, I. Trimaille, and S. Rigo, *J. Noncryst. Solids* (to be published).
- <sup>7</sup>E. H. Poindexter, P. Caplan, B. Deal, and R. Razouk, *J. Appl. Phys.* **52**, 879 (1981).
- <sup>8</sup>J. H. Stathis and L. Dori, *Appl. Phys. Lett.* **58**, 1641 (1991).
- <sup>9</sup>J. L. Cantin, M. Schoisswohl, H. J. von Bardeleben, N. H. Zoubir, and M. Vergnat, *Phys. Rev. B* **52**, 11 599 (1995).
- <sup>10</sup>A. Stesmans and V. V. Afanasev, *J. Appl. Phys.* **83**, 2449 (1998).
- <sup>11</sup>E. H. Poindexter and P. J. Caplan, *Prog. Surf. Sci.* **14**, 201 (1983).
- <sup>12</sup>K. Brower, *Appl. Phys. Lett.* **43**, 1111 (1983).
- <sup>13</sup>V. Ya. Bratus, S. S. Ishchenko, S. M. Okulov, I. P. Vorona, H. J. von Bardeleben, and M. Schoisswohl, *Phys. Rev. B* **50**, 15 449 (1994).
- <sup>14</sup>J. L. Cantin, M. Schoisswohl, H. J. von Bardeleben, V. Morrazzani, J. J. Ganem, and I. Trimaille, in Ref. 1, p. 28.
- <sup>15</sup>J. H. Stathis, E. Cartier, A. H. Edwards, and E. H. Poindexter, in *Silicon Nitride and Silicon Oxide Thin Insulating Films* (Electrochemical Society, Pennington, NJ, 1997), p. 259.
- <sup>16</sup>A. Stesmans, B. Nouwen, and V. V. Afanas'ev, *Phys. Rev. B* **58**, 15 801 (1998).
- <sup>17</sup>A. Stesmans, *Semicond. Sci. Technol.* **4**, 1000 (1989).
- <sup>18</sup>A. Stesmans and G. van Gorp, *Phys. Rev. B* **39**, 2864 (1989).
- <sup>19</sup>A. Stesmans and G. van Gorp, *Phys. Rev. B* **52**, 8904 (1995).
- <sup>20</sup>S. Sitbon, M. C. Hugon, B. Agius, F. Abel, J. L. Courant, and M. Puech, *J. Vac. Sci. Technol. A* **13**, 2900 (1995).
- <sup>21</sup>R. P. Vasquez, M. H. Hecht, F. J. Grunthaler, and M. L. Naiman, *Appl. Phys. Lett.* **44**, 969 (1984).
- <sup>22</sup>K. Yamamoto and N. Nakazawa, *Jpn. J. Appl. Phys., Part 1* **33**, 285 (1994).
- <sup>23</sup>K. H. Hwang, E. Yoon, K. W. Whang, and J. Y. Lee, *Appl. Phys. Lett.* **67**, 3590 (1995).
- <sup>24</sup>J. L. Cantin, Ph.D. thesis, Université Paris 6 (1997).
- <sup>25</sup>V. Bratus, S. S. Ishchenko, S. M. Okulov, I. P. Vornova, and H. J. von Bardeleben, *Mater. Sci. Forum* **196-201**, 529 (1995).
- <sup>26</sup>A. Pasquarello, M. S. Hybertson, and R. Car, *Appl. Phys. Lett.* **68**, 625 (1996).
- <sup>27</sup>W. L. Warren, J. Kanicki, F. C. Rong, and E. H. Poindexter, *J. Electrochem. Soc.* **139**, 880 (1992).
- <sup>28</sup>N. Ishi, S. Oozora M. Kumeda, and T. Shimizu, *Phys. Status Solidi B* **114**, K111 (1982).
- <sup>29</sup>R. A. B. Devine, J. M. Francou, A. Inard, and J. Pelletier, *Appl. Phys. Lett.* **56**, 1549 (1990).
- <sup>30</sup>D. Jousse, J. Kanicki, and J. H. Stathis, *Appl. Surf. Sci.* **39**, 412 (1989).
- <sup>31</sup>S. Garcia, I. Martil, G. G. Gonzales Diaz, E. Castan, S. Duenas, and M. Fernandez, *J. Appl. Phys.* **83**, 332 (1998).
- <sup>32</sup>I. Odhomari, H. Akatsu, Y. Yamakoshi, and K. Kishimoto, *J. Appl. Phys.* **62**, 3751 (1987).
- <sup>33</sup>G. Lucovsky, Z. Ying, and D. R. Lee, *J. Vac. Sci. Technol. B* **14**, 2832 (1996).
- <sup>34</sup>D. T. Krick, P. M. Lenahan, and J. Kanicki, *J. Appl. Phys.* **64**, 3558 (1988).
- <sup>35</sup>M. C. Hugon, F. Delmotte, B. Agius, and J. L. Courant, *J. Vac. Sci. Technol. A* **15**, 3143 (1997).